

# Decentralized Vehicle Coordination: The Berkeley DeepDrive Drone Dataset

©The Author(s) 2022  
DOI: 10.1177/ToBeAssigned

Fangyu Wu<sup>1</sup>, Dequan Wang<sup>1</sup>, Minjune Hwang<sup>1</sup>, Chenhui Hao<sup>1</sup>, Jiawei Lu<sup>1</sup>, Jiamu Zhang<sup>1</sup>, Christopher Chou<sup>1</sup>, Trevor Darrell<sup>1</sup>, and Alexandre Bayen<sup>1</sup>

## Abstract

Decentralized multiagent planning has been an important field of research in robotics. An interesting and impactful application in the field is decentralized vehicle coordination in understructured road environments. For example, in an intersection, it is useful yet difficult to deconflict multiple vehicles of intersecting paths in absence of a central coordinator. We learn from common sense that, for a vehicle to navigate through such understructured environments, the driver must understand and conform to the implicit “social etiquette” observed by nearby drivers. To study this implicit driving protocol, we collect the *Berkeley DeepDrive Drone* dataset. The dataset contains 1) a set of aerial videos recording understructured driving, 2) a collection of images and annotations to train vehicle detection models, and 3) a kit of development scripts for illustrating typical usages. We believe that the dataset is of primary interest for studying decentralized multiagent planning employed by human drivers and, of secondary interest, for computer vision in remote sensing settings.

## Keywords

Decentralized multiagent planning, autonomous driving, remote sensing

## Introduction

Studying human behaviors such as driving, cycling, and walking is a key topic in autonomous driving and human-robot interaction. A necessary step to design and validate any human behavior models is empirical data collection. In this regard, camera is highly effective for 1) it is capable of capturing rich dynamics on roads at a relatively low cost, 2) it can be quantitatively assessed via direct inspection, and 3) it is amenable for qualitative analysis using computer vision.

Most of the existing camera datasets can be classified into either *body-framed* dataset or *inertia-framed* dataset. The body-framed datasets have cameras placed on the traffic participants, e.g., on top a survey vehicle, to observe the movements of the surrounding traffic. The inertia-framed datasets have cameras installed at some overhead positions above some roads of interest to observe all road occupants within its field of view.

Body-framed datasets are useful to study behaviors of the surrounding traffic participants with respect to the host. It is arguably the most commonly used method for autonomous driving perception research. Many well-known datasets fall within this category, such as the KITTI dataset Geiger et al. (2013), the Oxford RoboCar dataset Maddern et al. (2017), the Waymo Open dataset Sun et al. (2019), and the Wamo Open Motion dataset Ettinger et al. (2021). Nevertheless, the body-framed placement makes it difficult to study persistent traffic patterns within a fixed spatial range. Moreover, placing the sensors on a low-profile moving object also results in undesirable occlusion.

Inertia-framed datasets are better suited to observe traffic within a fixed spatial range. By construction, the inertial-framed placement makes it very easy to estimate the recorded vehicle and human movements with respect to

the ground. Because the cameras are often placed on a vantage point, occlusion is also not as problematic. In this category, we also find many seminal datasets, including the NGSIM dataset United States Federal Highway Administration (2016), the ARED dataset Wu et al. (2019a), the Stanford Drone dataset Robicquet et al. (2020), the highD dataset Krajewski et al. (2018), and the INTERACTION dataset Zhan et al. (2019).

Most of the existing datasets, including the ones mentioned above, focus solely on human behaviors in structured environments. Behaviors in *understructured* road environments, such as highways with collisions and unsignalized intersections, have rarely been surveyed. Yet, the behaviors of traffic participants in understructured environments are highly interesting.

Understanding how humans coordinate with each other, i.e., the implicit “social etiquette”, has profound impacts. It helps autonomous vehicles to mimic human drivers to navigate through understructured road environments. It may also inspire new designs of decentralized motion planning algorithms for autonomous vehicles and warehouse robots. The lack of data in this domain undoubtedly hinders its development. To bridge the gap in empirical data, we propose an inertial-framed dataset: the Berkeley DeepDrive Drone (B3D) dataset.

The main contribution of this work is this open-sourced dataset. It records rich dynamics of human driving behaviors

<sup>1</sup>University of California, Berkeley, US

### Corresponding author:

Fangyu Wu, 652 Sutardja Dai Hall, Berkeley, CA 94709, USA  
Email: fangywu@berkeley.edu

in understructured road environments, including unsignalized intersections, unsignalized roundabouts, highways with collisions, highways with stop-and-go waves, and highways with merging bottlenecks. To our best knowledge, it is the first inertia-framed dataset with extensive coverage on understructured driving behaviors.

The rest of the article is organized as follows. We describe the content of the dataset in Section *Dataset*. We present the details of data collection in Section *Data Generation*. We highlight two use cases in Section *Areas of Applications*. Lastly, we conclude our work in Section *Summary and Future Work*.

## Dataset

The dataset consists of 20 post-processed videos, 16002 annotated images, and a development kit. It can be accessed from <https://github.com/b3d-project/b3d>. The sizes of the videos, the annotated images, and the development kit are 84.5 GB, 1.55 GB, and 225 MB, respectively, totaling to about 86.3 GB. The file structure of the dataset is illustrated in Figure 1. We briefly describe the three dataset components below.

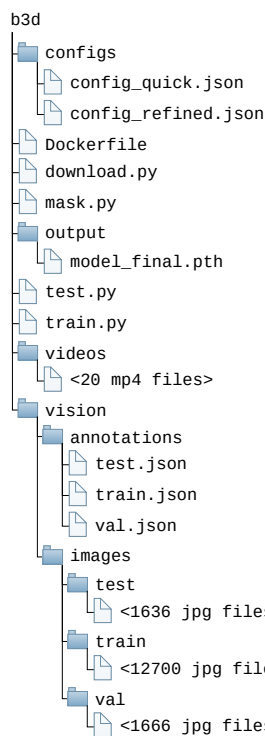


**Figure 1.** File structure of the B3D dataset. Informational files METADATA, LICENSE, and README are omitted for concision.

## Processed Videos

Among the 20 processed videos, eight were recorded on top of junctions and 12 on top of highways. An overview of the topology of the roads covered in the videos is illustrated in Figure 3. The videos are stored in mp4 format, which can be opened by all common video players.

Scenarios recorded in the video can be classified into the following six categories: 1) unsignalized intersections, 2)

unsignalized roundabouts, 3) tailgating accidents, 4) stop-and-go waves, 5) roadwork-induced merging, and 6) ramp-induced merging.

*Unsignalized intersections* can be found in videos jnc00.mp4, jnc01.mp4, jnc02.mp4, and jnc07.mp4. Videos jnc00.mp4 and jnc01.mp4 are two variants of three-way intersections, as shown in Figure 3a and Figure 3b, respectively. Videos jnc02.mp4 and jnc07.mp4 are two variants of four-way intersections, as shown in Figure 3c and Figure 3d, respectively.

*Unsignalized roundabouts* are captured in jnc03.mp4, jnc04.mp4, jnc05.mp4, and jnc06.mp4. Videos jnc03.mp4 and jnc04.mp4 are two recordings of a five-way roundabout, as shown in Figure 3e. Videos jnc05.mp4 and jnc06.mp4 are two variants of four-way roundabouts, as shown in Figure 3f and Figure 3g, respectively. Compared to video jnc03.mp4, video jnc04.mp4 has slightly more traffic.

The *tailgating accidents* consist of two collision events, first in hwy00.mp4 and then in hwy01.mp4. At 00:45 of hwy00.mp4, we observe the first accident near the left margin of the frame, as shown in Figure 2a. At 13:10 of hwy01.mp4, we find another traffic accident in the middle of the frame, as shown in Figure 2b. Video hwy02.mp4 captures the resulting congested traffic induced by the second incident. The timestamps of the collision events are visualized in Figure 4.

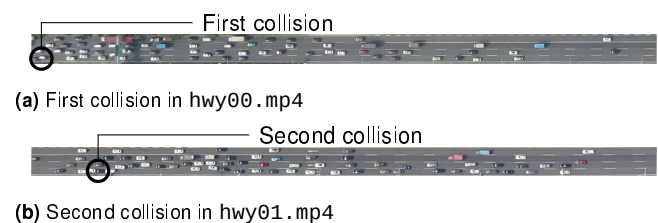


**Figure 2.** Tailgating collisions in hwy00.mp4 and hwy01.mp4. The collided vehicles are circled in black. The first accident involves at least two vehicles, while the second incident involves four vehicles.

*Stop-and-go waves* are recorded in hwy04.mp4 and hwy05.mp4. The first stop-and-go wave forms between 02:30 and 05:07 of hwy04.mp4. The second stop-and-go wave emerges between 06:06 and 08:10 of hwy04.mp4. The third stop-and-go wave is observed between 10:26 and 12:25 of hwy04.mp4. The fourth wave happens between 00:00 and 01:33 of hwy05.mp4. The last visible wave occurs between 05:19 and 06:07 of hwy05.mp4. For comparison, we provide video hwy03.mp4 as a free-flow baseline. The formation and dissipation events of the stop-and-go waves are visualized in Figure 5.

*Roadwork-induced merging* is recorded in hwy06.mp4, hwy07.mp4, and hwy08.mp4. The topology of the scenario is a four-lane-to-two-lane bottleneck, as shown in Figure 3j. Persistent congestion is observed before the merge point, while free-flow traffic is formed after the merge point.

*Ramp-induced merging* is recorded in hwy09.mp4, hwy10.mp4, and hwy11.mp4. The topology of the ramp is shown in Figure 3k, where a three-lane on-ramp is merging into a four-lane congested highway. The traffic stays congested *before and after* the merge point.

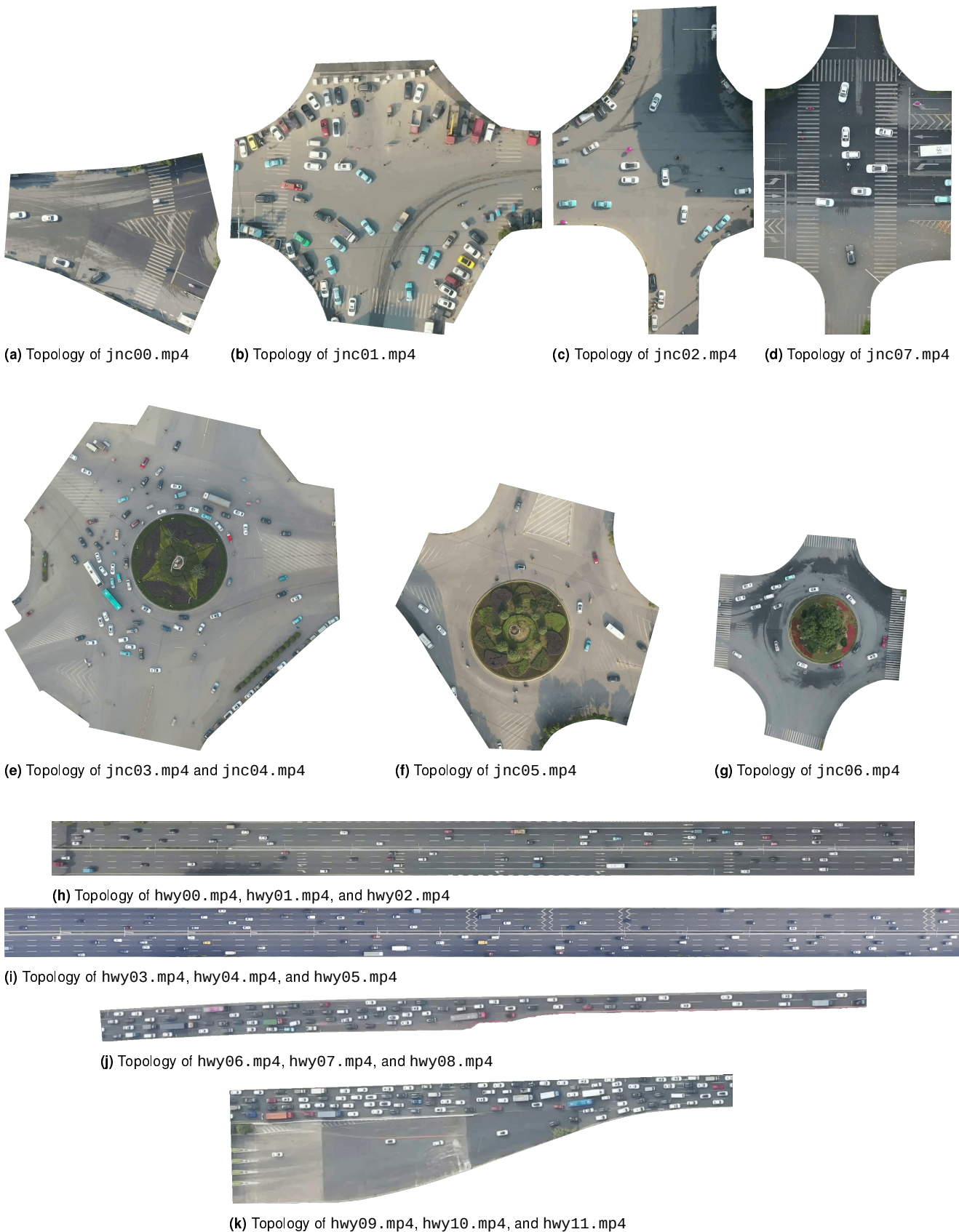


**Figure 3.** Typical Road Topology from the B3D dataset. In alphabetic order, we have (a)-(d) unsignalized intersections, (e)-(g) unsignalized roundabouts, (h)-(i) highways, and (j)-(k) merging bottlenecks. (a)-(d) are roughly on the same scale. (e)-(g) are on another identical scale. (h)-(i) are approximately on a third identical scale. Lastly, (j)-(k) are on a fourth distinct scale.

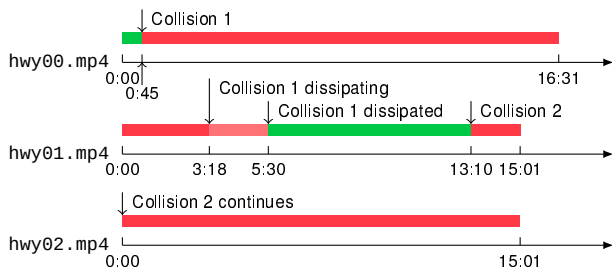


**Figure 4.** Timeline of the *tailgating accidents*. Green indicates regular traffic. Red indicates congestion caused by a collision. Light red indicates the induced congestion starts dissipating.

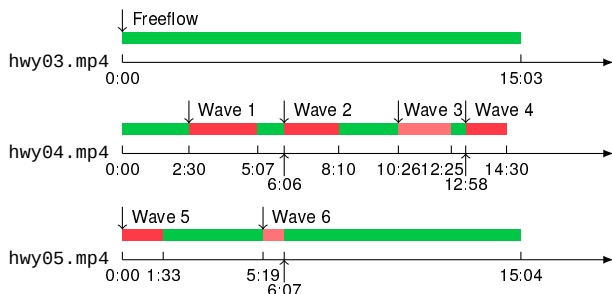


**Figure 5.** Timeline of the *stop-and-go* waves. Green indicates regular traffic. Red indicates congestion caused by a strong *stop-and-go* wave. Light red indicates congestion caused by a weak *stop-and-go* wave.

## *Annotated Images*

To qualitatively analyze the vehicle behaviors observed in the videos, it is necessary to obtain a precise trajectory of every relevant vehicle in the scene. To construct the trajectory of a vehicle, one common approach is to first detect its position in every frame and then to use a tracking algorithm to associate each detected position across frames.

To this end, we build an image dataset, which can be used to train a vehicle detection model. The dataset consists of 16002 annotated images, 80% of which is split for training, 10% of which for validation, and 10% of which for testing. An example annotation is shown in Figure 6.

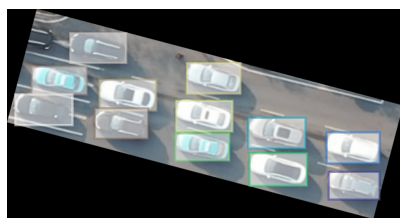


**Figure 6.** An example annotated image. Colored rectangles are axially aligned bounding boxes of the vehicles in the scene.

A total of 135303 bounding boxes are annotated for junction images and a total of 129939 bounding boxes created for highway images. Note that the annotations contain only one object class, that is, the *vehicle* class. We do not distinguish large vehicles, such as buses and trucks, from small vehicles, such as sedans and SUVs.

To inspect or edit the provided annotations, we recommend using the open source annotation tool Computer Vision Annotation Tool (CVAT) [Sekachev et al. \(2020\)](#).

*Development Kit*

In addition to the videos and the annotated images, we provide a development kit consisting of three example scripts: `train.py`, `test.py`, and `mask.py`.

Among them, the script `train.py` is used to show how the annotated image data may be used to train a neural network model for vehicle detection. In this script, we use the object detection library Detectron2 [Wu et al. \(2019b\)](#) to train a RetinaNet model [Lin et al. \(2017\)](#) for detecting locations of vehicles in an input image.

The script `test.py` applies the trained model, trained via the `train.py` script, to an input image. This script is intended to serve as an example for post-training evaluation and inference. For convenience, we provide an optional pre-trained model, which can be used directly for inference. This way, users can directly use a working detection model without having to go through the computationally expensive training step locally. An instance of the detection results using the pre-trained model is shown in Figure 7.



**Figure 7.** An example image with detection results. Colored rectangles are axially aligned bounding boxes. Black numbers are confidence scores of the estimated bounding boxes, with 1.0 being full certainty and 0.0 being full uncertainty.

Finally, we provide a masking script `mask.py` that crops an image according to a pre-defined polygonal mask. For example, Figure 8 shows how the script crops off irrelevant part of the roundabout image according to the red mask. The script intends to help users to focus on the only relevant part of the scene, where relevance is defined by the user via CVAT. To crop a video, one only needs to define a polygonal mask for *one* frame of a video and then apply masking to *every* frame of the video.

For reproducibility, we encapsulate the development environment in a Docker image. The image can be directly built from the provided Dockerfile.

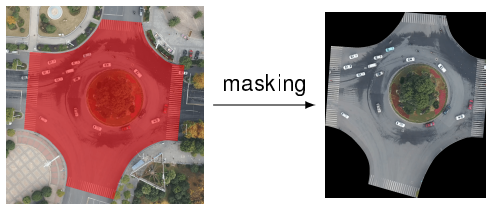


**Figure 8.** A demonstration of the masking process. The red polygonal mask is defined via CVAT. Pixels outside of the mask are considered irrelevant and are marked as black.

## Data Generation

In this section, we briefly describe how the data was generated, including 1) how the videos were collected and processed and 2) how the image annotations were created.

### Video Collection and Processing

The 20 aerial videos were recorded with a DJI Mavic 2 Pro quadcopter between December 11 and December 21 of 2019 in China. Specific dates, lengths, and locations of the shootings are tabulated in Table 1.

During each video shooting, we positioned the quadcopter directly above the road of interest and keep the quadcopter hovering as long as the battery permitted. A top-view video was then recorded at 4K and 30 FPS using the built-in camera. An visualization of the experiment setup is shown in Figure 9. Due to limited battery capacity, each shooting was limited between 15 and 20 minutes.

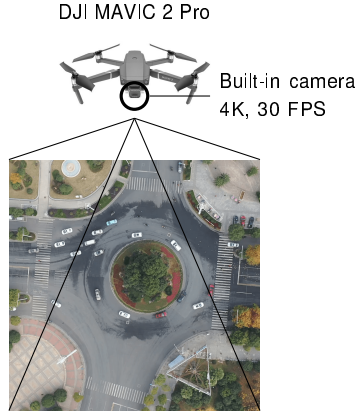


**Figure 9.** An illustration of the experiment setup. The quadcopter hovers over the road of interest, during which the built-in camera records the top-view of each traffic participant as they go in and out of the scene.

After data collection, the raw videos were additionally filtered through a post-processing procedure, including compression, normalization, stabilization, and trimming. In particular, all junction videos were normalized to an uniform scale of 20.825 pixel/meter, while all highway videos normalized to another scale of 6.667 pixel/meter.

### Image Annotation

To train a neural network model for vehicle detection, we manually cropped and labeled 16002 images. We cropped candidate images from the 20 videos by first extracting one frame every 15 seconds and then manually labelling an

**Table 1.** Dates, Lengths, and Locations of Videos

Name	Date	Length	Location
jnc00	11Dec19 10:34:49	21:31.13	(27.682343, 111.434406)
jnc01	11Dec19 11:12:24	21:31.33	(27.700318, 111.436217)
jnc02	11Dec19 11:54:14	18:47.90	(27.691014, 111.430694)
jnc03	13Dec19 16:08:34	20:02.67	(27.758277, 111.997546)
jnc04	13Dec19 16:34:26	21:01.80	(27.758274, 111.997575)
jnc05	14Dec19 14:34:13	20:29.87	(27.748028, 111.986952)
jnc06	15Dec19 14:59:56	20:47.62	(26.905471, 112.553030)
jnc07	15Dec19 16:21:29	20:55.42	(26.896411, 112.573248)
hwy00	20Dec19 10:39:47	16:31.26	(23.195657, 113.365076)
hwy01	20Dec19 11:04:03	15:01.90	(23.195657, 113.365076)
hwy02	20Dec19 11:27:21	15:01.80	(23.195657, 113.365076)
hwy03	20Dec19 15:31:57	15:03.84	(23.180680, 113.367367)
hwy04	20Dec19 15:54:14	14:30.87	(23.180680, 113.367367)
hwy05	20Dec19 16:20:23	15:04.77	(23.180680, 113.367367)
hwy06	21Dec19 12:38:35	17:01.46	(23.107395, 113.345787)
hwy07	21Dec19 13:01:55	17:02.66	(23.107395, 113.345787)
hwy08	21Dec19 13:26:57	18:01.18	(23.107395, 113.345787)
hwy09	21Dec19 15:08:24	16:00.83	(23.103120, 113.345733)
hwy10	21Dec19 15:32:38	15:30.80	(23.103120, 113.345733)
hwy11	21Dec19 15:58:53	10:45.21	(23.103120, 113.345733)

axially aligned bounding box to each vehicle in the selected frames. Next, we cropped around significant vehicle clusters in each frame, generating the final annotated image dataset.

We note that this labeling-then-cropping approach is important for space efficiency and detection efficacy. Clearly, the cropping helps reduce the size of candidate images by removing irrelevant part of the frames such as trees, rooftops, and parking lots. This is especially helpful for training on GPUs, since typically graphics cards have smaller memory compared to that of system RAMs. Moreover, cropping ensures that candidate images are of regular proportion. This is important for the region proposal step of vehicle detection. If we did not crop the frames and applied the trained model directly on elongated frames like those in Figure 2, we would get very low detection accuracy due to inaccurate region proposal.

## Areas of Applications

We believe that the dataset is useful in wide spectrum of applications in robotics. Specifically, we present two impactful use cases: one in motion planning and another in computer vision.

The primary area of applications is to model behaviors of human driving in understructured environments for decentralized motion planning. A typical modeling procedure may be as follows: 1) run the masking script to select relevant part of the video dataset; 2) apply the detection model to extract position of each vehicle in the masked scene; 3) inspect the results of the detection and, if necessary, manually correct any detection errors; 4) use a tracking algorithm such as SORT [Bewley et al. \(2016\)](#) to associate detected positions into trajectories; and 5) learn and validate a human driving model based on the estimated trajectories. An accurate human behavior model may be deployed on autonomous vehicles for navigation in understructured road environments. Additionally, the resulting model may serve as a baseline to develop decentralized coordination algorithms for other robotics applications such as warehouse robots.

The secondary use case is to develop or to evaluate computer vision algorithms for small road occupants in remote sensing settings. An accurate pedestrian and cyclist detection method enables us to study rich interactions among different modes of transportation without needing a labor-intensive process of human annotation. To our best knowledge, detecting pedestrians or cyclists from aerial videos remains a challenge for the state-of-the-art computer vision. This is largely due to low resolution of those small objects, because low resolution renders the objects visually ambiguous, as illustrated in Figure 10. It is plausible that a detection model may find it challenging to distinguish a pedestrian from a watermark, as shown in Figure 10a and Figure 10b, or to discern two pedestrians from a cyclist, as shown in Figure 10c and Figure 10d. To this end, our dataset may serve as a data source to build training data and to validate candidate algorithms.



**Figure 10.** Visual ambiguity of low resolution objects. (a)(b) are visually alike. (c)(d) are also visually similar.

## Summary and Future Work

In this article, we present the Berkeley DeepDrive Drone dataset. The dataset contains a total of 20 processed videos, 16002 annotated images, and a development kit. It may be used in various applications, including but not limited to: 1) modeling driver behaviors in understructured road environments, 2) designing decentralized motion planning algorithms, and 3) developing detection methods for low-resolution road occupants. Future work includes estimating trajectories of vehicles and other traffic participants in the videos and expanding the video repository to include other phenomena in understructured road environments.

## Acknowledgements

This work is funded in part by the Berkeley DeepDrive at the University of California, Berkeley. We would like to express our gratitude to Zhixiong Huang, Junjie Zou, and Kewen Liao for their generous supports on the logistics aspect of the data collection.

## References

- Bewley A, Ge Z, Ott L, Ramos F and Upcroft B (2016) Simple online and realtime tracking. In: *IEEE International Conference on Image Processing*. pp. 3464–3468. DOI:10.1109/ICIP.2016.7533003.
- Ettinger S, Cheng S et al. (2021) Large scale interactive motion forecasting for autonomous driving: The waymo open motion dataset. In: *Proceedings of the IEEE/CVF International Conference on Computer Vision*. pp. 9710–9719.
- Geiger A, Lenz P, Stiller C and Urtasun R (2013) Vision meets robotics: The kitti dataset. *International Journal of Robotics Research* 32(11): 1231–1237.
- Krajewski R, Bock J, Kloeker L and Eckstein L (2018) The hignd dataset: A drone dataset of naturalistic vehicle trajectories on german highways for validation of highly automated driving systems. In: *International Conference on Intelligent Transportation Systems*. pp. 2118–2125. DOI:10.1109/ITSC.2018.8569552.
- Lin TY, Goyal P, Girshick R, He K and Dollár P (2017) Focal loss for dense object detection. In: *Proceedings of the IEEE International Conference on Computer Vision*. pp. 2980–2988.
- Maddern W, Pascoe G, Linegar C and Newman P (2017) 1 Year, 1000km: The Oxford RobotCar Dataset. *The International Journal of Robotics Research* 36(1): 3–15. DOI:10.1177/0278364916679498. URL <http://dx.doi.org/10.1177/0278364916679498>.
- Robicquet A, Sadeghian A, Alahi A and Savarese S (2020) Learning social etiquette: Human trajectory prediction in crowded scenes. In: *European Conference on Computer Vision*, volume 2.
- Sekachev B, Manovich N et al. (2020) opencv/cvat: v1.1.0. DOI: 10.5281/zenodo.4009388. URL <https://doi.org/10.5281/zenodo.4009388>.
- Sun P, Kretzschmar H et al. (2019) Scalability in perception for autonomous driving: Waymo open dataset DOI:10.48550/ARXIV.1912.04838. URL <https://arxiv.org/abs/1912.04838>.
- United States Federal Highway Administration (2016) Next generation simulation (ngsim) vehicle trajectories and supporting data. URL <http://doi.org/10.21949/1504477>.
- Wu F, Stem RE, Cui S, Delle Monache ML, Bhadani R, Bunting M, Churchill M, Hamilton N, Piccoli B, Seibold B et al. (2019a) Tracking vehicle trajectories and fuel rates in phantom traffic jams: Methodology and data. *Transportation Research Part C: Emerging Technologies* 99: 82–109.
- Wu Y, Kirillov A, Massa F, Lo WY and Girshick R (2019b) Detectron2. URL <https://github.com/facebookresearch/detectron2>.
- Zhan W, Sun L, Wang D et al. (2019) INTERACTION Dataset: An INTERnational, Adversarial and Cooperative motion Dataset in Interactive Driving Scenarios with Semantic Maps. *arXiv:1910.03088 [cs, eess]*.